Helsinki University of Technology, Institute of Mathematics, Research Reports
Teknillisen korkeakoulun matematiikan laitoksen tutkimusraporttisarja
Espoo 2005 A485

BAYESIAN APPROACH TO DETECTION OF ANOMALIES IN ELECTRICAL IMPEDANCE TOMOGRAPHY

Sampsa Pursiainen

TEKNILLINEN KORKEAKOULU
TEKNISKA HÖGSKOLAN
HELSINKI UNIVERSITY OF TECHNOLOGY
TECHNISCHE UNIVERSITÄT HELSINKI
UNIVERSITE DE TECHNOLOGIE D'HELSINKI

Helsinki University of Technology, Institute of Mathematics, Research Reports
Teknillisen korkeakoulun matematiikan laitoksen tutkimusraporttisarja
Espoo 2005 A485

BAYESIAN APPROACH TO DETECTION OF ANOMALIES IN ELECTRICAL IMPEDANCE TOMOGRAPHY

Sampsa Pursiainen

Helsinki University of Technology
Department of Engineering Physics and Mathematics
Institute of Mathematics

Sampsa Pursiainen: *Bayesian approach to detection of anomalies in electrical impedance tomography*; Helsinki University of Technology, Institute of Mathematics, Research Reports A485 (2005).

Abstract: *The electrical impedance tomography problem is to estimate an unknown conductivity distribution of a given object from a set of static electric measurements on the boundary. In this study, the problem is formulated in terms of Bayesian statistics by treating the conductivity distribution within the object as a random variable with some posterior probability distribution and by employing Markov chain Monte Carlo sampling methods for exploring the properties of this distribution. The goal is to develop such an algorithm that finding a proper numerical solution would necessitate as small amount of computational work as possible. MCMC based estimates are compared to least-squares reconstructions. Numerical experiments concentrate on a special case where a relatively small perturbation is sought from otherwise constant conductivity distribution. To summarize the findings, it is often difficult to obtain any appropriate reconstruction which is due to the non-linearity and the strong ill-conditioned nature of the inverse problem. The statistical model is preferable to the least-squares approach only if there is accurate enough prior information available. Accuracy of both least-squares and statistical solutions can be improved through an enhanced model of voltage measurement errors which is based on Monte Carlo sampling of the prior density.*

AMS subject classifications: 65N21, 65C05, 65F05

Keywords: electrical impedance tomography, Bayesian statistics, Markov chain Monte Carlo, linear algebra, anomalous conductivities

Correspondence

Sampsa.Pursiainen@hut.fi

ISBN 951-22-7637-2
ISSN 0784-3143

Helsinki University of Technology
Department of Engineering Physics and Mathematics
Institute of Mathematics
P.O. Box 1100, 02015 HUT, Finland
email:math@hut.fi http://www.math.hut.fi/

1 Introduction

The *electrical impedance tomography* (EIT) problem is to estimate an unknown conductivity distribution of a given object Ω from a set of static electricmeasurements on the boundary $\partial\Omega$. The problem was first introduced in a rigorous mathematical form by A. P. Calderón in [6]. We consider in this article the *complete electrode model*, where the voltage data is generated by injecting electrical currents to the object through a set of contact electrodes attached on the boundary and measuring the resulting voltage values on the electrodes. For a review on EIT see [8].

Potential applications of EIT are numerous. In medical imaging [5] these include detection and classification of tumors from breast tissue [15, 9, 22, 39, 28] and measuring brain function [30, 10]. Industrial applications include topics such as imaging of fluid flows and mixing in process pipelines [34, 32, 35, 17, 11] and non-destructive testing of materials [38, 21].

In this work, the EIT problem is formulated in terms of *Bayesian statistics* by treating the conductivity distribution within the object as a random variable with some *posterior probability distribution* and by employing *Markov chain Monte Carlo* (MCMC) sampling methods for exploring the properties of this distribution. We focus on detection of a small perturbation (anomaly) from the background conductivity distribution. The objective is to assess conditions under which the numerical solution is feasible. We discuss also Monte Carlo schemes that are computationally efficient. Drawing a random sample from the posterior distribution requires solving the *forward problem*, which can be approximated as a system of linear equations. Therefore, we are interested in finding an effective linear algebraic method for the forward problem. Moreover, we consider a *surrogate forward solution*, i.e. a method that does not necessitate solving the linear system, and how such a method can be applied to speed up the MCMC sampling process. Statistical solutions are compared to least-squares reconstructions. The implemented least-squares algorithm is the *regularized quasi-Newton method*. There are numerous papers that consider anomalous conductivities in electrical impedance tomography, e.g. [1], [3] and [2]. For a review on statistical inversion and MCMC methods in EIT see [19].

Mathematical models of the forward and the inverse problems, the quasi-Newton method and the Bayesian formulation of the inverse problem are briefly reviewed in section 2 by following the presentation of [19]. The end of the section introduces the *enhanced likelihood model*, where the idea is to improve the model of voltage measurement errors through MCMC integration.

Section 3 introduces MCMC methods. We describe shortly the general idea of MCMC integration and three MCMC sampling algorithms: the *Metropolis-Hastings algorithm*, *random-walk metropolis* and the *surrogate transition method*.

In section 4, we show how the forward solution can be updated by using the *Sherman-Morrison-Woodbury formula* and estimate what is the corresponding

amount of computational work.

Numerical experiments are performed in section 5. In the demonstrated problem a circular anomaly is sought from a unit disc. Quasi-Newton reconstructions are obtained by applying a *smoothness regularization* technique that is based on the *finite element method* (FEM) and has been developed by the authors. The MCMC based estimation scheme is experimented by running random-walk Metropolis with different prior assumptions. Feasibility of the surrogate transition method is experimented by generating a sampling run where the posterior probability is evaluated through the surrogate forward solution. In the section 5.4, the enhanced likelihood model is applied both to the quasi-Newton optimization method and Monte Carlo integration based estimation.

In section 6 we discuss the results of the numerical experiments and directions for further study.

2 The EIT problem

In stationary EIT a *current pattern* $I = (I_1, \ldots, I_L)$, that is a set of electrical currents, is applied to the object Ω through a set of contact electrodes $\{e_\ell\}_{\ell=1}^L$ on its boundary $\partial\Omega$. The resulting *voltage pattern* $U = (U_1, \ldots, U_L)$ is measured with the same electrodes. The conductivity distribution within the object $\sigma : \Omega \to \mathbb{R}$, independent of time, is reconstructed from a number of such measurements.

2.1 The forward problem

We consider a model where σ is real-valued and strictly positive function in Ω and corresponding to each σ there is u is a scalar voltage potential in Ω satisfying the equation

$$\nabla \cdot (\sigma \nabla u) = 0 \tag{1}$$

and the boundary conditions

$$\int_{e_\ell} \sigma \frac{\partial u}{\partial n}\, dS = I_\ell, \quad 1 \le \ell \le L, \tag{2}$$

$$\sigma \frac{\partial u}{\partial n}\Big|_{\partial\Omega \setminus \cup e_\ell} = 0, \tag{3}$$

$$u + z_\ell \sigma \frac{\partial u}{\partial n} = U_\ell, \quad 1 \le \ell \le L, \tag{4}$$

where $z = (z_1, \ldots, z_L)$ is a vector containing the contact impedances between the electrodes and the object. Additionally, the injected currents are supposed to satisfy the charge conservation condition and the ground voltage is chosen so

that the sum of electrode potentials is zero. Hence, the we require that

$$\sum_{\ell=1}^{L} I_\ell = 0 \qquad \text{and} \qquad \sum_{\ell=1}^{L} U_\ell = 0. \tag{5}$$

The forward problem is to solve the pair (u, U) from the above equations corresponding to given σ, I and z.

2.2 Numerical solution of the forward problem

The forward problem is solved numerically by applying finite element method [4] to the *weak form* of (1)-(5). It has been shown in [36] that the solution of the weak form exists and is unique in $H^1(\Omega) \oplus \mathbb{R}^L$.

Partition of Ω is obtained by decomposing its polygonal approximation into a *shape regular* set of triangles $\mathcal{T}_h = \{T_1, \ldots, T_M\}$. The subindex h indicates the mesh size. The discrete conductivity distribution σ_h is assumed to be constant in each triangle, i.e. $\sigma_h \in \text{span}\{\chi_{T_m} \,|\, 1 \le m \le M\}$, where χ_{T_m} is the characteristic function of T_m. Consequently, σ_h has as many degrees of freedom as there are triangles in $\mathcal{T}_h$. In further discussion, we identify σ_h with a vector in $\mathbb{R}^M$.

Ritz-Galerkin approximation u_h of the potential field u is sought from a finite-dimensional space which is spanned by the piecewise linear *nodal basis* $\{\varphi_1, \ldots, \varphi_n\}$, that is a set of piecewise linear functions where each basis function differs from zero precisely at one of the nodes of $\mathcal{T}_h$.

The numerical solution of the forward problem is the pair (u_h, U_h) with the representations

$$u_h = \sum_{i=1}^{n} \alpha_i \varphi_i \qquad \text{and} \qquad U_h = \mathcal{C}\beta, \tag{6}$$

where $\alpha = (\alpha_1, \ldots, \alpha_n)^T \in \mathbb{R}^n$, $\beta = (\beta_1, \ldots, \beta_{L-1})^T \in \mathbb{R}^{L-1}$ and $\mathcal{C}$ in which the entries $\mathcal{C}_{i,i} = 1$ and $\mathcal{C}_{i,j+1} = -1$ for $i, j = 1, \ldots, L$ differ from zero. With this choice the sum of the electrode voltages is equal to zero. Applying the Ritz-Galerkin method to the weak form of (1)-(5) yields a system of linear equations (see [37]):

$$\begin{pmatrix} B & C \\ C^T & G \end{pmatrix} \begin{pmatrix} \alpha \\ \beta \end{pmatrix} = \begin{pmatrix} 0 \\ \mathcal{C}^T I \end{pmatrix}, \tag{7}$$

where

$$B_{i,j} = \int_\Omega \sigma \nabla \varphi_i \cdot \nabla \varphi_j \, dx + \sum_{\ell=1}^{L} \frac{1}{z_\ell} \int_{e_\ell} \varphi_i \varphi_j \, dS, \tag{8}$$

$$C_{i,j} = -\frac{1}{z_1} \int_{e_1} \varphi_i \, dS + \frac{1}{z_{j+1}} \int_{e_{j+1}} \varphi_i \, dS, \tag{9}$$

$$G_{i,j} = \begin{cases} |e_1|/z_1, & \text{for} \quad i \neq j \\ |e_1|/z_1 + |e_{j+1}|/z_{j+1}, & \text{for} \quad i = j. \end{cases} \tag{10}$$

2.3 The inverse problem

To solve the finite dimensional EIT *inverse problem* is to estimate the unknown conductivity distribution on the basis of the voltage measurements on the boundary.

The voltage data does not uniquely determine the unknown: in real-life applications the conductivity distribution may have infinite number of degrees of freedom whereas the number of measurements is always finite. The inverse problem is also *ill-conditioned*, i.e. small changes to the measured voltages may cause very large changes to the solution. Roughly, this is due to the fact that the equation (1) is essentially a diffusion equation where $\sigma(x)$ is the diffusivity at x: a local perturbation of σ causes only a slight but, still, global perturbation of u, which may be hardly distinguishable on the boundary.

The measured voltages are assumed to be noisy. In our model the noise in the measurements is additive Gaussian white noise and independent of σ, which means that the measurements V and the true potential values on the electrodes U are linked through formula

$$V = U(\sigma) + N,$$

where N is distributed as $\mathcal{N}(0, \gamma_N^2 I)$.

Voltage data consists of $L-1$ voltage patterns $V^{(1)}, \ldots, V^{(L-1)}$ which correspond to $L-1$ linearly independent current patterns $I^{(1)}, \ldots, I^{(L-1)}$. The independency must be required, since the right hand side of the weak form of (1)-(5) is linear with respect to I. Again, the maximal number of linearly independent patterns is $L-1$, which is due to the charge conservation constraint $\sum_{\ell=1}^{L} I_\ell = 0$. Matrices that contain all $L-1$ voltage patterns stacked together are denoted with the symbols

$$\mathbf{U}(\sigma) = \begin{pmatrix} U^{(1)}(\sigma) \\ \vdots \\ U^{(L-1)}(\sigma) \end{pmatrix} \qquad \text{and} \qquad \mathbf{V} = \begin{pmatrix} V^{(1)} \\ \vdots \\ V^{(L-1)} \end{pmatrix}.$$

Solving $\mathbf{U}(\sigma)$ numerically requires for solving the linear system (11) with respect to each current pattern $I^{(1)}, \ldots, I^{(L-1)}$. The problem can be formulated as

$$A_\sigma X_\sigma = F, \tag{11}$$

where A_σ is the matrix described in (7), (8)-(10) and the number of columns in X_σ and F is $L-1$. The ith column of F is the right hand side of (7) constructed with respect to the ith current pattern.

2.3.1 Current patterns

We use trigonometric current patterns which are given by the formula

$$I_\ell^{(k)} = \begin{cases} I_{\max}\cos(k\theta_\ell), & 1 \le \ell \le L,\ 1 \le k \le \frac{L}{2}, \\ I_{\max}\sin((k - L/2)\theta_\ell), & 1 \le \ell \le L,\ \frac{L}{2} < k \le L-1, \end{cases} \tag{12}$$

where the constant $I_{\max}$ denotes the amplitude of the current. $\theta_\ell = 2\pi\ell/L$ is the angular location of the midpoint of electrode e_ℓ and k is the spatial frequency. These are *optimal current patterns* [18, 7] to distinguish a centered rotation invariant annulus from a homogenous disc with respect to the metric $\mathrm{dist}(\sigma_1, \sigma_2) = ||U(\sigma_1) - U(\sigma_2)||/||I||$.

2.4 Numerical solution of the inverse problem

We implement two complementary ways to solve the EIT inverse problem in terms of Bayesian statistics: Markov Chain Monte Carlo integration and least-squares approximation.

Bayesian statistics allows describing various uncertainties in the model as probability distributions and, therefore, provides a coherent way to approach the inverse problem. The disadvantage of Bayesian approach is that even though setting up the probability model is not difficult drawing appropriate estimates from the resulting probability distribution is often problematic and computationally expensive.

2.4.1 The Bayesian model

Bayesian formulation of the EIT inverse problem is a simple application of the well-known *Bayes formula*:

$$\pi_{post}(\sigma) = \pi(\sigma \mid \mathbf{V}) = \pi_{pr}(\sigma)\pi_{lh}(\mathbf{V} \mid \sigma),$$

where $\pi_{pr}(\sigma)$ is the *prior density* which contains all the prior information of the conductivity distribution and $\pi_{lh}(\mathbf{V}|\sigma)$ is the *likelihood density* that is the conditional probability of measuring $\mathbf{V}$. A product of these two densities is, up to a scaling, the posterior density $\pi_{post}(\sigma)$ which describes a probability distribution for the unknown variables.

In this work, we use a simple subset constraint the prior density

$$\pi_{pr}(\sigma) = \chi_{S_{pr}}(\sigma)/|S_{pr}|, \tag{13}$$

where $\chi_{S_{pr}}$ is the characteristic function of the set $S_{pr} \subset \mathbb{R}^M$ that is chosen based on prior knowledge of the true conductivity distribution. This is due to the simplicity of the numerically demonstrated problem. In real-life applications it is typically not enough just to restrict the problem to some subspace, but

more sophisticated prior distributions have to be applied, e.g. regularizing priors favoring anomalies of certain size.

The model of additive Gaussian white noise $\mathbf{N} = \mathbf{V} - \mathbf{U}(\sigma)$ implies that the likelihood probability of measuring $\mathbf{V}$ is

$$\pi_{lh}(\mathbf{V} \mid \sigma) \propto \exp\Big(-\frac{1}{2\gamma_N^2}(\mathbf{U}(\sigma) - \mathbf{V})^T(\mathbf{U}(\sigma) - \mathbf{V})\Big). \tag{14}$$

The posterior density, which is the *Bayesian solution* of the present inverse problem, is a product of (13) and (14). An estimate of the true conductivity distribution can be found by estimating some property of the posterior distribution. In this work, we are interested in estimating the *posterior expectation* (or conditional mean estimate)

$$\int_{\mathbb{R}^M} \sigma \pi_{post}(\sigma) d\sigma. \tag{15}$$

Unfortunately, examining the posterior distribution numerically is problematic whenever the dimension of the problem is large enough. Estimation of the posterior expectation requires for evaluation of the integral (15) but it is a well-known fact that standard numerical quadratures are infeasible for large dimensional domains. Therefore, we employ Markov chain Monte Carlo integration which is an extensively used strategy in Bayesian computations.

2.4.2 The regularized quasi-Newton method

In least-squares approximation the idea is to minimize the likelihood norm $||\mathbf{U}(\sigma) - \mathbf{V}||^2$ by applying some regularization method and by linearizing the map $\sigma \to \mathbf{U}(\sigma)$. A typical example of a minimization method that is based on linearization is the classical Newton's method. Least-squares methods are popular being typically easily implemented and computationally relatively cheap.

The following quasi-Newton algorithm employs *generalized Tikhonov regularization*. That is, the minimized functional is

$$\Phi_\alpha(\sigma) = \frac{1}{2}||\mathbf{U}(\sigma) - \mathbf{V}||_W^2 + \frac{\alpha}{2}A(\sigma),$$

where $A(\sigma)$ is the regularizing functional, $\alpha > 0$ is the regularization parameter and

$$||\mathbf{U}(\sigma) - \mathbf{V}||_W^2 = \sum_{k=1}^{K}\sum_{l=1}^{L} w_{k,l}(U_\ell^{(k)}(\sigma) - V_\ell^{(k)})^2. \tag{16}$$

W is a symmetric positive definite weight matrix. $\Phi_\alpha(\sigma)$ is minimized through the following iterative gradient-based optimization process

$$\sigma^{(i+1)} = \sigma^{(i)} - \lambda_s^{(i)} H_\alpha(\sigma^{(i)})^{-1}\nabla\Phi_\alpha(\sigma^{(i)}), \tag{17}$$

$$H_\alpha(\sigma^{(i)}) = D\mathbf{U}(\sigma^{(i)})^T W D\mathbf{U}(\sigma^{(i)}) + \frac{1}{2}\alpha D^2 A(\sigma^{(i)}) \tag{18}$$

$$\nabla\Phi_\alpha(\sigma^{(i)}) = D\mathbf{U}(\sigma^{(i)})^T W(\mathbf{U}(\sigma^{(i)}) - \mathbf{V}) + \frac{1}{2}\alpha D A(\sigma^{(i)}). \tag{19}$$

where $D\mathbf{U}(\sigma^{(i)})$ is a differential and $H_\alpha(\sigma^{(i)}) \in \mathbb{R}^{M\times M}$ is a regularized Hessian matrix of the map $\sigma \to \mathbf{U}(\sigma)$, $DA(\sigma^{(i)})$ is a differential of the map $\sigma \to A(\sigma)$ and $\lambda_s^{(i)} > 0$ is a relaxation parameter controlling the step size.

Note that the logarithm of (14) coincides with (16) up to a constant with the choice $W = I$. Therefore, the quasi-Newton method yields a *maximum posterior* (MAP) estimate, i.e. an estimate of the location of the maximum of the posterior density, in which the prior density is defined by the regularizing functional.

Unfortunately, implementing the quasi-Newton algorithm by applying any regularization method favoring strongly discontinuous conductivities, such as anomalies of certain size and shape, is problematic. Therefore, we implement the method by applying a regularization technique that produces smooth conductivities. Another difficulty is that least-squares algorithms do not have a strict statistical interpretation. For that reason, estimating reliability of least-squares reconstructions is difficult.

2.4.3 The enhanced likelihood model

Suppose that $\mathbf{U}^*(\sigma)$ is some numerical approximation of $\mathbf{U}(\sigma)$. Then, $\mathbf{V}$ can be written as

$$\mathbf{V} = \mathbf{U}(\sigma) + \mathbf{N} = \mathbf{U}^*(\sigma) + (\mathbf{U}(\sigma) - \mathbf{U}^*(\sigma)) + N,$$

where the second term is the modeling error. Due to the fact that there is always some approximation error in the numerically computed electrode potentials it is evident that there must be more consistent models for the likelihood density than (14) that does not take the approximation error into account.

Therefore, we experiment the enhanced likelihood model introduced in [20] where $\mathbf{U}^*(\sigma) - \mathbf{V}$ is supposed to be distributed as $\mathcal{N}(\mu, \Gamma)$ where μ and Γ are the conditional expectation and the conditional covariance of the approximation error with respect to the prior distribution. That is,

$$\mu = \int (\mathbf{U}^*(\sigma) - \mathbf{U}(\sigma))\pi_{pr}(\sigma)d\sigma, \tag{20}$$

$$\Gamma = \int (\mathbf{U}^*(\sigma) - \mathbf{U}(\sigma) - \mu)(\mathbf{U}^*(\sigma) - \mathbf{U}(\sigma) - \mu)^T \pi_{pr}(\sigma)d\sigma + \gamma_N^2 I. \tag{21}$$

Naturally, these integrals have to be estimated numerically, which, again, can be done by employing MCMC methods.

Due to the fact that it is often difficult to encode prior knowledge to the regularizing functional we also experiment enhancing the performance of the quasi-Newton method by weighing the least-squares norm (16) with the inverse of the conditional covariance of $\mathbf{U}(\sigma)$ by choosing the weight matrix as

$$W^{-1} = \int (\mathbf{U}(\sigma) - \mu)(\mathbf{U}(\sigma) - \mu)^T \pi_{pr}(\sigma)d\sigma + \gamma_N^2 I, \tag{22}$$

where $\mu = \int \mathbf{U}(\sigma)\pi_{pr}(\sigma)d\sigma$. With this choice $\exp(-\frac{1}{2}||\mathbf{U}(\sigma)-\mathbf{V}||^2_W)$ is a Gaussian approximation of the posterior density.

3 Markov chain Monte Carlo integration

The basic formula in MCMC integration is the *Monte Carlo approximation*,

$$\frac{1}{m}\sum_{i=1}^{m} f(x^{(i)}) \approx \int_{\mathbb{R}^n} f(x)\pi(x)dx, \tag{23}$$

where $\{x^{(i)}\}_{i=1}^{\infty}$ is an *ergodic Markov Chain* with a *transition function* $P : \mathbb{R}^n \times \mathbb{R}^n \to \mathbb{R}^n$ and *equilibrium distribution* π. The validity of (23) is based on the *law of large numbers* and the *central limit theorem*, the proofs of which can be found from [29]. The law of large numbers guarantees that the estimation (23) is valid with large m and the central limit theorem shows that the approximation error is of order $O(m^{-1/2})$ and independent of the dimensionality of the state space. For that reason, MCMC methods are suitable for large dimensional integration problems.

In contrast to the traditional Markov chain analysis where one is typically given the transition function and is interested in knowing what the stationary distribution is, in Markov chain Monte Carlo simulations, one knows the equilibrium distribution and is interested in prescribing an efficient transition rule so as to reach the equiblirium. According to [25], variance of the approximation error can be estimated as

$$\mathrm{var}\Big\{\frac{1}{m}\sum_{i=1}^{m} f(x^{(i)}) - \int_{\mathbb{R}^n} f(x)\pi(x)\,dx\Big\} \approx \frac{1}{m}\mathrm{var}\{f\}\Big(1 + 2\sum_{j=1}^{\infty}\rho_j\Big),$$

where $\rho_j = \mathrm{corr}\{f(x^{(1)}), f(x^{(j+1)})\}$, i.e. the less there is correlation between consecutive states of the chain the more reliable estimates are obtained. In an optimal case, the chain would produce independent samples directly from π. Therefore, the transition function $P(x, y)$ should be in some sense close to $\pi(y)$. That is, the transition function should be adapted to follow the dynamics of the equilibrium distribution and such that the ith state $x^{(i)}$, becomes rapidly nearly independent of the starting state $x^{(0)}$ as i increases.

Due to the great success MCMC methods have achieved in solving multidimensional integration and optimization problems numerous MCMC algorithms have been developed in many different fields which include physics, statistics, chemistry and structural biology. However, it is important to emphasize that finding an ideal chain is more an art than a mathematically solvable problem. In practice, one always tends to feel unsatisfied in settling down on any chain. In this work, we introduce the well-known Metropolis-Hastings algorithm, random-walk Metropolis and the surrogate transition method following the presentation of [25].

3.1 The Metropolis-Hastings algorithm

The Metropolis-Hastings algorithm [26, 16] is based on a 'trial - and - error' strategy. It uses a proposal function $T(x, y)$ to suggest a possible move from x to y and then through an acceptance-rejection rule ensures that the target distribution π is the equilibrium distribution of the resulting Markov chain.

Algorithm 3.1 (Metropolis-Hastings)

- *Given the current state* $x^{(t)}$ *and a proposal function* $T(x, y)$ *that satisfies* $T(x, y) > 0$ *if and only if* $T(y, x) > 0$.
- *Draw* y *from the proposal distribution* $T(x^{(t)}, y)$.
- *Draw* $U \sim$ *Uniform*$[0, 1]$ *and update*

$$x^{(t+1)} = \begin{cases} y, & if U \leq r(x^{(t)}, y) \\ x^{(t)} & otherwise \end{cases}$$

where

$$r(x, y) = \min\left\{1, \frac{\pi(y)T(y, x)}{\pi(x)T(x, y)}\right\}.$$

Apparently, choice of the proposal function has a great effect on the convergence rate, which is why the Metropolis-Hastings algorithm is useful in many connections; it does not set serious restrictions on the proposal probability.

3.1.1 Random-walk Metropolis

The random-walk Metropolis algorithm is based on perturbing the current configuration $x^{(t)}$ by adding a random error so that the proposed candidate position is $y = x^{(t)} + \epsilon$ where ϵ is identically distributed for all t and such that the range of the exploration can be controlled by the user. When one does not have much information about the structure of the equilibrium distribution, ϵ is often drawn from a spherically symmetric Gaussian distribution $\mathcal{N}(0, \gamma_T^2 I)$. With this choice the algorithm is:

Algorithm 3.2 (Random-walk Metropolis)

- *Given the current state* $x^{(t)}$
- *Draw* $\epsilon \sim \mathcal{N}(0, \gamma_T^2 I)$ *and set* $y = x^{(t)} + \epsilon$. *The variance* γ_T^2 *is chosen by the user.*
- *Simulate* $U \sim$ *Uniform*$[0, 1]$ *and update*

$$x^{(t+1)} = \begin{cases} y, & if U \leq \frac{\pi(y)}{\pi(x^{(t)})} \\ x^{(t)} & otherwise \end{cases}$$

It has been suggested in [33] that γ_T^2 should be chosen so that a 25% to 35% acceptance rate is maintained. Despite of the fact that the Metropolis-Hastings algorithm (3.1) allows one to use asymmetric proposal functions, a simple random-walk proposal is still most frequently seen in practice, since finding a good proposal transition kernel is often difficult.

3.2 The surrogate transition method

It is typical in Monte Carlo simulations that evaluation of $\pi(x)$ involves expensive computation, although it is cheap to obtain a relatively good approximation $\pi^*(x) \approx \pi(x)$. Such is the case in the present statistical inverse problem, where each evaluation of the posterior density requires solving the numerical forward problem (11) but it is often sufficient to only approximate the solution through a linearized model

$$\mathbf{U}^*(\sigma) = \mathbf{U}(\sigma_0) + D\mathbf{U}(\sigma_0)(\sigma - \sigma_0). \tag{24}$$

where $D\mathbf{U}(\sigma)$ is the Jacobian matrix of the map $\sigma \to \mathbf{U}(\sigma)$. This technique has been successfully applied in [19]. In this work, we call (24) the surrogate forward solution and introduce the surrogate transition method [25, 24] where the idea is to speed up the calculations without biasing the equilibrium density by defining a surrogate transition rule based on the approximation $\pi^*(x)$.

Suppose one can conduct a *reversible* Markov transition $S(x, y)$ leaving π^* invariant, i.e. the *detailed balance* condition $\pi^*(x)S(x, y) = \pi^*(y)S(y, x)$ is satisfied. The surrogate transition rule can be defined by using the Metropolis-Hastings principle on π^*:

Algorithm 3.3 (Surrogate transition method)

- *Given a current sample* $x^{(t)}$.
- *Let* $y_0 = x^{(t)}$ *and recursively*

  $$y_i \sim S(y_{i-1}, \cdot),$$

  for $i = 1, \ldots, k$.
- *Update* $x^{(t+1)} = y_k$ *with probability*

  $$\min\left\{1, \frac{\pi(y_k)/\pi^*(y_k)}{\pi(x^{(t)})/\pi^*(x^{(t)})}\right\}$$

  and let $x^{(t+1)} = x^{(t)}$ *with the remaining probability.*

If $\pi^*(x)$ is easily evaluated and close enough to $\pi(x)$ this will arguably speed up the sampling procedure since $\pi^*(x)$ is evaluated k times more often than $\pi(x)$ during the algorithm.

4 Linear algebra

Since the computational cost required for evaluation of the posterior density $\pi_{post}(\sigma)$ is mainly concentrated in solving the numerical forward problem, performance of the implemented MCMC algorithm depends highly on the applied linear algebraic methods.

In this section, we show how the matrix of the linear system (11) is updated in the sampling process and how the solution can be corrected by applying the Sherman-Morrison-Woodbury formula [13] after each update.

4.1 Updating the system matrix

Let t be a real number and d a vector in $\mathbb{R}^M$ such that $d_{j_\ell} = 1$ for m indices $1 \leq j_1, \ldots, j_m \leq M$ and $d_j = 0$ otherwise. Suppose the conductivity distribution $\sigma \in \mathbb{R}^M$ is updated as $\sigma \to \sigma + td$. This corresponds to a rank k update to the system matrix A_σ:

$$A_{\sigma+td} = A_\sigma + tV_d\Lambda_d V_d^T, \tag{25}$$

where $V_d = (e_{i_1}, e_{i_2}, \ldots, e_{i_k})$ is formed by k canonical basis vectors $(e_i)_j = 1$ for $j = i$ and $(e_i)_j = 0$ for $i \neq j$ and Λ_d is a symmetric and positive definite $k \times k$-matrix satisfying $(\Lambda_d)_{j\ell} = \int_\Omega \nabla\varphi_{i_j} \cdot \nabla\varphi_{i_\ell}\, dx$. The updated indices $i_1, \ldots, i_k$ coincide with those nodes of $\mathcal{T}_h$ that intersect with the support of the update. Typically, k is a relatively small number. For instance, $k = 3$ if σ is updated only in one triangle.

4.1.1 The reduced system

Suppose that X_σ is known and $X_{\sigma+td}$ is to be solved. Using the representation (25) the linear system (11) can be written as

$$X_{\sigma+td} = X_\sigma - t(A_\sigma + tV_d\Lambda V_d^T)^{-1}V_d\Lambda_d V_d^T X_\sigma. \tag{26}$$

We see that $X_{\sigma+td}$ can easily be obtained if the solution of $(A_\sigma + tV_d\Lambda_d V_d^T)Z_{\sigma,d,t} = V_d$ is known. The number of columns in $Z_{\sigma,d,t}$ is k whereas $X_{\sigma+td}$ has $L-1$ columns. If k is less than $L-1$ it might be preferable to solve $Z_{\sigma,d,t}$ instead of $X_{\sigma+td}$. The advantage is particularly notable if an iterative solver is applied to the forward problem, since iterative methods solve a multicolumn system column by column but we show below that $Z_{\sigma,d,t}$ is useful also if the sampler operates only in a small subset of the object Ω.

4.2 The Sherman-Morrison-Woodbury formula

Let A be an invertible real $N \times N$ matrix, U_1, U_2 be real $N \times k$ matrices and let $I + U_2^T A^{-1} U_1$ be invertible. Then, a straightforward multiplication shows that

$$(A + U_1U_2^T)^{-1} = A^{-1} - A^{-1}U_1(I + U_2^T A^{-1}U_1)^{-1}U_2^T A^{-1}, \tag{27}$$

i.e. a rank k correction to the matrix A causes a rank k correction to its inverse.

Suppose that σ is strictly positive vector and t and d are chosen so that $\sigma + td$ is again a strictly positive vector. By choosing $A = A_\sigma$, $U_1 = tV_d\Lambda_d$ and $U_2 = V_d$ the matrices $A + U_1U_2^T = A_\sigma + tV_d\Lambda_dV_d^T$ and $I + U_2^TA^{-1}U_1 = I + tV_d^TA_\sigma^{-1}V_d\Lambda_d$ are invertible, which can be shown as follows.

Due to the strict positiveness of $\sigma + td$, the matrix $A_{\sigma+td}$ is positive definite. Furthermore, we can choose $s > \max\{-t, 0\}$ so that $\sigma - sd$ is a strictly positive vector. Thus, we can write $A_{\sigma+td} = A_{\sigma-sd} + (s+t)V_d\Lambda_dV_d^T$, where $A_{\sigma+td}$, $A_{\sigma-sd}$ and Λ_d are positive definite matrices, i.e.

$$\begin{aligned} x^T(\Lambda_d^{-1} + tV_d^TA_\sigma^{-1}V_d)x &= x^T(\Lambda_d^{-1} + (t+s)V_dA_{\sigma-sd}^{-1}V_d)x \\ &= x^T\Lambda_d^{-1}x + (t+s)(V_dx)^TA_{\sigma-sd}^{-1}(V_dx) \\ &> 0, \end{aligned}$$

for all $x \neq 0$. Since s was chosen so that $s+t > 0$, we see that the left hand side is positive definite. Consequently, we can write the inverse of $(I + tV_d^TA_\sigma^{-1}V_d\Lambda_d)^{-1}$ as a product of Λ_d^{-1} and $(\Lambda_d^{-1} + tV_d^TA_\sigma^{-1}V_d)^{-1}$ and the inverse of $A_{\sigma+td}$ can be written as

$$A_{\sigma+td}^{-1} = A_\sigma^{-1} - tA_\sigma^{-1}V_d\Lambda_d(I + tV_d^TA_\sigma^{-1}V_d\Lambda_d)^{-1}V_d^TA_\sigma^{-1} \quad . \tag{28}$$

4.2.1 Restriction to a submatrix

Multiplying the equation (28) from right by V_d, applying the notation introduced in section (4.1.1) and denoting $Z_{\sigma,d} = Z_{\sigma,d,0}$ yields

$$Z_{\sigma,d,t} = Z_{\sigma,d} - tZ_{\sigma,d}(I + tV_d^TZ_{\sigma,d}\Lambda_d)^{-1}V_d^TZ_{\sigma,d}.$$

In other words, it is easy to compute $Z_{\sigma,d,t}$ if $Z_{\sigma,d}$ is known. Furthermore, multiplying (28) from right by F results into

$$X_{\sigma+td} = X_\sigma - tZ_{\sigma,d}(I + tV_d^TZ_{\sigma,d}\Lambda_d)^{-1}V_d^TX_\sigma.$$

and we see that by knowing $Z_{\sigma,d}$ one is able to directly correct the solution X_σ. Suppose now that one does contiguous updates $\sigma_1 \to \sigma_1 + t_1d_1 = \sigma_2 \to \sigma_2 + t_2d_2 = \sigma_3 \to \ldots$ such that the vectors d_i for all i are supported in some subspace of $\mathbb{R}^M$ which correspond to a K dimensional subset of the nodal basis and let $D = (e_{i_1}, e_{i_2}, \ldots, e_{i_K})$ be a collection of canonical basis vectors that span this subset. By multiplying the equation (28) from right by D and by denoting $Z_{\sigma,D} = A_\sigma^{-1}D$ we have

$$Z_{\sigma+td,D} = Z_{\sigma,D} - tZ_{\sigma,d}(I + tV_d^TZ_{\sigma,d}\Lambda_d)^{-1}V_d^TZ_{\sigma,D}. \tag{29}$$

Due to the fact that D is a submatrix of an identity matrix, $Z_{\sigma,D}$ is a submatrix of $A_{\sigma_D}^{-1}$. Moreover, V_d is a submatrix of D which implies that $Z_{\sigma,d}$ is submatrix of $Z_{\sigma,D}$. Thus, one knows each of the matrices Z_{σ,d_i} if one knows $Z_{\sigma,D}$.

Briefly, it is enough to do all the computations with $A_\sigma^{-1}D$ which is a submatrix of A_σ^{-1} provided that all the conductivity updates are restricted into a subset of Ω that corresponds to D.

4.2.2 Computational work

Suppose that the rank k of the update $A_\sigma + V_d\Lambda_d V_d^T$ is much smaller than the number of rows N. Then, it is preferable to compute first the inverse of the full $k \times k$ -matrix $\Lambda_d(I + tV_d^T A^{-1}V_d)$, which is known to take not more than $O(k^3)$ floating point operations. Taking into account that evaluating $A_\sigma^{-1}V_d$ is equivalent to just picking k columns from A_σ^{-1} we conclude that the product

$$\underset{k\times N}{T_1} = \underset{k\times k}{[\Lambda_d(I + tV_d^T A_\sigma^{-1}V_d\Lambda_d)^{-1}]}\,\underset{k\times N}{[V_d^T A_\sigma^{-1}]}$$

requires evaluating k^2N separate multiplications of floating-point values and $k(k-1)N$ additions, that is, $O(k(2k-1)N)$ flops as a whole. Similarly, computing the product

$$\underset{N\times N}{T_2} = t\,\underset{N\times k}{[A_\sigma^{-1}V_d]}\;\underset{k\times N}{[T_1]}$$

requires for $O((2k-1)N^2)$ operations. Finally, in the summation

$$\underset{N\times N}{(A_\sigma + tV_d\Lambda_d V_d^T)^{-1}} = \underset{N\times N}{A_\sigma^{-1}} + \underset{N\times N}{T_2}$$

N^2 entries are added together which takes $O(N^2)$ operations.

The computational effort of updating the inverse matrix by employing the Sherman-Morrison-Woodbury formula (28) is, consequently, of magnitude

$$O(k^3) + O(2k^2N) + O(2kN^2) + O(N^2) \sim O(2kN^2). \tag{30}$$

Operating with the whole inverse matrix is practically never reasonable which is due to the large number of non-zero entries. In the Sherman-Morrison-Woodbury formula, the columns of A_σ^{-1} are processed independently. Supposing that only K columns are updated the computational effort (30) is decreased by the factor K/N. For that reason, the effort of evaluating $Z_{\sigma,D}$ in (29) is of order $O(2kKN)$ which is small with small k and K.

5 Numerical experiments

In this section, we demonstrate how the introduced methods are applied to the EIT problem. The idea is more to describe phenomena that occur when solving the inverse problem numerically than to strictly simulate any real application. Therefore, the experimental setup is as simple as possible.

In the present experiments, the computations are performed in a polygonal approximation of the unit disc $B(0,1)$. There are sixteen electrodes ($L = 16$) evenly distributed along the boundary curve together covering approximately 50 % of the total length. The contact impedances and the current patterns are normalized so that $z_1 = \ldots = z_L = 1$ and $I^{(1)}_{max} = \ldots = I^{(L-1)}_{max} = 1$.

5.1 Small perturbations

We seek a small circular perturbation (anomaly) from Ω. The exact conductivity distribution $\sigma^{ex} \in \mathcal{A}(\Omega)$ is assumed to be of the form,

$$\sigma^{ex} = \sigma^{ex}_{bg} + \delta^{ex}, \tag{31}$$

where σ^{ex}_{bg} is the background conductivity distribution satisfying $\sigma_{bg}(x) = 1$ for all $x \in \Omega$ and δ^{ex} is a perturbation function that attains the value $\delta^{ex}(x) = t$ in a disc $B(\mathbf{c}, r)$ and is otherwise equal to zero. $\mathbf{c} = (c_1, c_2) \in \mathbb{R}^2$ and $r, t \in \mathbb{R}$ are unknown constants. Within this notation the inverse problem is simply to find out the quadruple c_1, c_2, r, t. We denote

$$\sigma^{ex} \widehat{=} \begin{pmatrix} c_1 & c_2 & r & t \end{pmatrix}. \tag{32}$$

Note that this model cannot be exactly implemented. Due to the fact that the discrete conductivity distribution is constant in each triangle the true distribution has to be interpolated in the framework of the triangulation.

An imaginable real life application analogous to this scheme could be detecting a tumor from breast tissue, where the background conductivity is close to a constant.

5.1.1 Setup

The triangulation $\mathcal{T}_h = \{T_m\}_{m=1}^M$ that is used in the following computations consists of 1476 nodes, 2659 triangles and 291 boundary edges (Figure 1). Due to the fact that variation of the potential distribution is most frequent in the

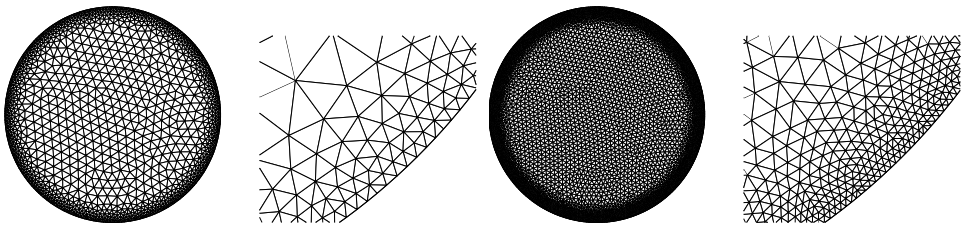

Figure 1: The triangulation $\mathcal{T}_h$ (left) and the refined mesh $\mathcal{T}_{h/2}$ (right), which is used in generating the data $\mathbf{V}$.

vicinity of the electrodes the triangulation is refined towards the boundary with respect to an exponential *distance function* .

In the present experiments, the exact conductivity distribution is

$$\sigma^{ex} \widehat{=} (0.5, 0.2, 0.1, -0.9).$$

The potential values $\mathbf{U}(\sigma^{ex})$ are computed by solving the numerical forward problem with respect to a distribution that is a piecewise constant interpolation of σ^{ex} within a refined triangulation (Figure 1) $\mathcal{T}_{h/2}$ which is obtained simply by dividing each triangle in $\mathcal{T}_h$ into four subtriangles. The applied piecewise constant interpolation is such that the interpolation function coincides with the interpolated function in the set of circumcenters of $\mathcal{T}_h$. The notation σ^{ex} can as well be regarded as referring to this interpolation illustrated in Figure 2. The simulated measurements are generated by adding Gaussian white noise $\mathbf{N} \sim \mathcal{N}(0, 10^{-6}I)$ to the numerically computed data. That is, $\mathbf{V} = \mathbf{U}(\sigma^{ex}) + \mathbf{N}$. This corresponds to a measurement error of magnitude

$$\frac{||\mathbf{N}||_2}{||\mathbf{V}||_\infty} \approx 0.2\%, \qquad \text{and} \qquad \frac{||\mathbf{N}||_2}{||\mathbf{U}(\sigma^{ex}) - \mathbf{U}(\sigma^{ex}_{bg})||_2} \approx 5\%. \tag{33}$$

The data is generated in the refined mesh, since otherwise we would be likely to find 'too good' candidate solutions. Using the same mesh in both generating the data and solving the inverse problem is known as committing an *inverse crime*. The approximation error between the meshes $\mathcal{T}_h$ and $\mathcal{T}_{h/2}$ is measured as

$$\frac{||\mathbf{U}(\sigma_{bg}) - \mathbf{U}(\sigma^{ex}_{bg})||_2}{||\mathbf{U}(\sigma^{ex}) - \mathbf{U}(\sigma^{ex}_{bg})||_2} \approx 29\%. \tag{34}$$

This is large compared to the error measurement error. However, the approximation error is a highly correlated error term. It is also obvious that whenever the sought anomaly is small enough the approximation error is likely be large. In this case reducing the approximation error considerably would necessitate a significant refinement to the triangulation.

5.2 The quasi-Newton reconstruction

So as to get some idea of the solutions that can be obtained through the least-squares approach, we compute a least-squares reconstruction by performing one step of the quasi-Newton iteration using the background conductivity σ_{bg} as an initial guess. The weight matrix in (16) is chosen to be the identity matrix. In general, taking more steps seldom leads to considerably better estimates. In this connection, taking one step seems to be enough.

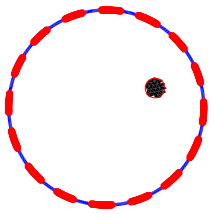

Figure 2: The piecewise constant interpolation of $\sigma^{ex} \widehat{=} (0.5, 0.2, 0.1, -0.9)$ in $\mathcal{T}_{h/2}$. The red circle denotes the right size and location of the anomaly.

5.2.1 Computation of the Jacobian Matrix

The Jacobian matrix $J_{i,j} = \frac{\partial U^{(i)}}{\partial \sigma_j}$ is computed by differentiating both sides of the equation (11) with respect to mth component which yields $\frac{\partial A_\sigma}{\partial \sigma_m} F + A_\sigma \frac{\partial F}{\partial \sigma_m} = 0$. Using the relation $X_\sigma = A_\sigma^{-1} F$, we obtain

$$\frac{\partial F}{\partial \sigma_m} = -A^{-1} \frac{\partial A}{\partial \sigma_m} F \qquad \text{and} \qquad \frac{\partial A}{\partial \sigma_m} = \begin{pmatrix} -\sigma_m^2 K_{T_m} & 0 \\ 0 & 0 \end{pmatrix}, \tag{35}$$

where K_{T_m} is the stiffness matrix with respect to the triangle T_m, i.e. $(K_{T_m})_{ij} = \int \chi_m \nabla\varphi_i \cdot \nabla\varphi_j \, dxdy$. The kth voltage pattern $U^{(k)}$ is obtained as $U^{(k)} = (0, \mathcal{C}) F^{(k)}$. Differentiating this and using (35) yields

$$\frac{\partial U^{(k)}}{\partial \sigma_m} = -\begin{pmatrix} 0 & \mathcal{C} \end{pmatrix} A_\sigma^{-1} \frac{\partial A_\sigma}{\partial \sigma_m} F^{(k)}. \tag{36}$$

Since there is no sense in evaluating a whole inverse matrix the Jacobian is computed by first evaluating the products $A_\sigma^{-1} \begin{pmatrix} 0 & \mathcal{C}^T \end{pmatrix}$ and $A_\sigma^{-1} F$ after which the partial derivatives are given by (36).

5.2.2 Smoothness regularization

In the quasi-Newton method regularization techniques favoring smooth conductivities are often the most successful ones. We apply a regularizing functional of

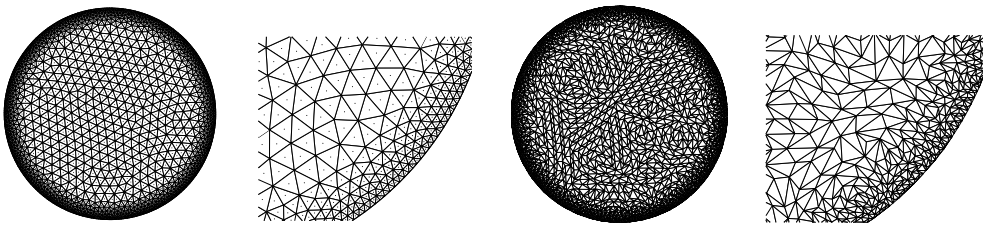

Figure 3: The set of circumcenters of the triangulation $\mathcal{T}_h$ (left) and the corresponding Delaunay triangulation $\mathcal{T}_h^d$.

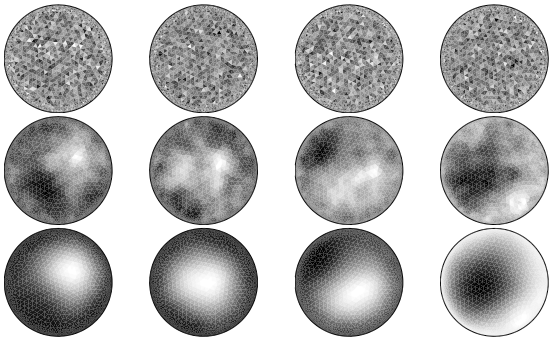

Figure 4: Four realizations of W (1th row) and the realizations of $X = K^{-k/2}W$ corresponding to $k = 2$ (2nd row), $k = 4$ (3rd row).

the form

$$\Psi(\sigma) = ||\sigma||^2_{K^k} = \sigma^T K^k \sigma, \tag{37}$$

where K^k, is the kth exponent of the stiffness matrix $K \in \mathbb{R}^{M\times M}$,

$$(K)_{ij} = \begin{cases} \int_\Omega \nabla\varphi_i^d \cdot \nabla\varphi_j^d \, dxdy, & \text{dist}(\text{supp}\{\varphi_i^d + \varphi_j^d\}, \partial\Omega) \geq \epsilon \\ \delta_{ij}, & \text{otherwise,} \end{cases}$$

where δ_{ij} is the Kronecker's delta and $\{\varphi_1^d, \ldots, \varphi_M^d\}$ is the piecewise linear nodal basis of a Delaunay triangulation $\mathcal{T}_h^d$ (i.e. a set of triangles such that no data points are contained in any triangle's circumcircle) that is generated with respect to the nodal basis formed by the set of circumcenters of the triangulation $\mathcal{T}_h$. This is illustrated in Figure 3. The submatrix of K that corresponds to the circumcentres close to the boundary is an identity matrix, which is a zero boundary condition for σ and verifies that K is positive definite. The boundary condition is added because the measured voltages are much less sensitive to the values of σ in the central parts of Ω than to the values close to the boundary $\partial\Omega$. In other words, sensitivity to the measurement noise increases when moving towards the center of Ω. Achieving feasible results with high noise levels seems to necessitate increasing 'stiffness' of the regularization in the vicinity of the electrodes.

A matrix similar to K is obtained as a result of FEM discretion of Laplace's equation with Dirichlet boundary condition. For that reason, we should have $||\nabla\sigma|| \sim ||\sigma||_K$; that is, the regularization method should favor smooth structured conductivities. This is indeed true and can be verified as follows.

Due to the fact that K is positive definite there is a constant of ellipticity α satisfying $\sigma^T K\sigma = \alpha||\sigma||^2$. Each σ has an uniquely determined piecewise linear counterpart $\sigma^d = \sum_{m=1}^M \sigma_m^d \varphi_m^d$ such that $\sigma - \sigma^d$ vanishes in the set of circumcenters of $\mathcal{T}_h$. By identifying σ and σ^d as vectors in $\mathbb{R}^M$ we have $(\sigma_1, \ldots, \sigma_M) = (\sigma_1^d, \ldots, \sigma_M^d)$

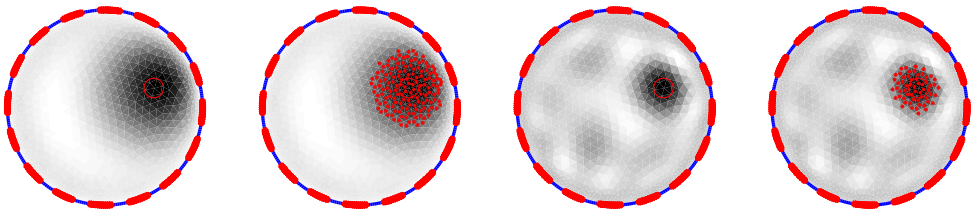

Figure 5: Quasi-Newton reconstructions corresponding to $\alpha = 10^{-1}$ (1st from left) and $\alpha = 10^{-5}$ (3rd). In both cases, the region of interest is determined as in (39) with $\kappa = 2.2$ (2nd and 4th).

and

$$\begin{aligned} ||\sigma||_K &= \sum_{m,\ell=1}^{M} \sigma_m \sigma_\ell \int \nabla\varphi_m^d \cdot \nabla\varphi_\ell^d \, dxdy \\ &= \sum_{m,\ell=1}^{M} \sigma_m^d \sigma_\ell^d \int \nabla\varphi_m^d \cdot \nabla\varphi_\ell^d \, dxdy = ||\nabla\sigma^d||^2. \end{aligned}$$

Hence, it is ok to call (37) smoothness regularization. Furthermore, we can write

$$||\sigma||_{K^k}^2 = \Big(\sum_m^M c_m z_m\Big)^T \Big(\sum_\ell^M c_\ell \lambda_\ell^k z_\ell\Big) = \sum_m^M \lambda_m^k c_m^2, \tag{38}$$

where $\lambda_1, \ldots, \lambda_M$ are the eigenvalues and $z_1, \ldots, z_M$ are the corresponding eigenvectors. By substituting $\alpha^{-k}K^k$ into (38) and by noticing that $\lambda_\ell \geq \alpha$ for $l = 1, \ldots, M$, we can deduce that $\alpha^{-t/2}||\sigma||_{K^t} \geq \alpha^{-s/2}||\sigma||_{K^s}$ for $t \geq s$, i.e. $||\sigma||_{K^k}$ increases when k increases. For that reason, the larger is the value of k the stronger is the smoothing effect of the regularization.

So as to demonstrate the structures generated by this regularization method, we draw *white noise* random samples $W \in \mathbb{R}^M, W \propto \mathcal{N}(0, I)$ and set $X = K^{-k/2}W$. Then,

$$||W||^2 = W^T W = X^T K^{k/2} K^{k/2} X = X^T K^k X = ||X||_{K^k}^2.$$

Random draws are plotted in Figure 4.

5.2.3 Results

The quasi-Newton method seems to give rather credible information about the location of the anomaly but the exact size and value of conductivity remain uncertain. The reconstructions corresponding to $\alpha = 10^{-1}$ and $\alpha = 10^{-5}$ are plotted in Figure 5. In both cases, the power k in the regularization function

(37) is equal to one. Decreasing the value of the regularization parameter leads to better localization of the anomaly but also to increased level of the overall variation of σ.

Since least-squares reconstructions are easily computed and seem to localize the anomaly relatively confidentially, we use least-squares approximation as a method of determining a *region of interest* that is a subset $\mathcal{R}_{pr} \subset \Omega$ in which the anomaly lies with high reliability.

The region of interest is determined as

$$\mathcal{R}_{pr} = \{x \in \Omega \,:\, |\sigma(x) - \sigma_{bg}(x)| \geq \kappa \,\mathrm{std}\{\sigma\}\}, \tag{39}$$

where σ is the quasi-Newton reconstruction, $\mathrm{std}\{\sigma\}$ its standard deviation and $\kappa > 0$ some real-valued constant. This appears to work pretty well in practice.

5.3 MCMC integration

Statistical solution refers in this case to a Monte Carlo approximation of the conditional expectation

$$\overline{\sigma}_m = \frac{1}{m}(\sigma^{(1)} + \cdots + \sigma^{(m)}) \approx \int_{\mathbb{R}^M} \sigma \pi_{post}(\sigma)\, d\sigma \tag{40}$$

In practice, achieving an reasonably accurate Monte Carlo estimate requires for heavy computation compared to least-squares approximation. Therefore, statistical solutions should be at least in some sense more precise than the corresponding least-squares solutions. Again, the applied sampling techniques and linear algebraic methods have a significant effect on the convergence rate and thereby the usability of this approach.

5.3.1 Prior and posterior densities

We hypothesize that the anomaly is of the form (31) and is located somewhere in the region of interest $\mathcal{R}_{pr}$ that is obtained from a quasi-Newton reconstruction as described in (39) and Figure 5. In other words, we hypothesize that the conductivity distribution can be written as in (32), where $r, \mathbf{c}$ and t are realizations of random variables and $\mathbf{c} \in \mathcal{R}_{pr}$. We do not assume anything particular of the shape of the prior distribution (e.g. Gaussian distribution), and therefore, let these random variables be independent and uniformly distributed.

Note that this prior model cannot be exactly implemented. Due to the fact that each conductivity distribution is constant in each triangle we cannot draw samples exactly distributed as π_{pr} but we have to apply the piecewise constant interpolation introduced in section 5.1.1.

Since the problem is restricted as (32), the integration task (40) is actually only four dimensional and MCMC integration is not necessarily needed. However,

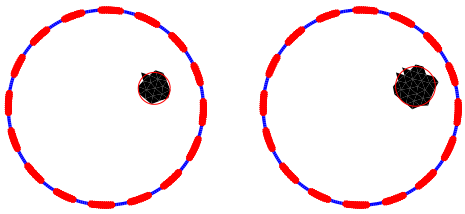

Figure 6: Two piecewise constant interpolation functions of random draws from π_{pr}. The red circle shows the exact size and shape of each perturbation.

a similar sampling scheme for the anomaly is workable also in more complex cases where the background conductivity σ_{bg} has to be included into the list of unknown variables.

5.3.2 Linear algebra

As the computations are restricted to the region of interest, each sampled conductivity can be represented as $\sigma = \sigma_{bg} + td$ so that the number of non-zeros in d is relatively small. Therefore, it is advantageous to solve the forward problem through the Sherman-Morrison-Woodbury -formula, introduced in section 4.2, as

$$X_\sigma = X_{\sigma_{bg}} - tZ^d_{\sigma_{bg}}(I + tV_d^T Z^d_{\sigma_{bg}}\Lambda_d)^{-1}V_d^T X_{\sigma_{bg}},$$

where the number of columns in $Z_{\sigma_{bg}}$ is the number of nodes in the region of interest. Since we correct each time the background solution $X_{\sigma_{bg}}$, the computational workload can be diminished by directly correcting each current pattern

$$U^{(i)}(\sigma) = U^{(i)}(\sigma_{bg}) - t \begin{pmatrix} 0 & \mathcal{C} \end{pmatrix} Z^d_{\sigma_{bg}}(I + tV_d^T Z^d_{\sigma_{bg}}\Lambda_d)^{-1}V_d^T X^{(i)}_{\sigma_{bg}},$$

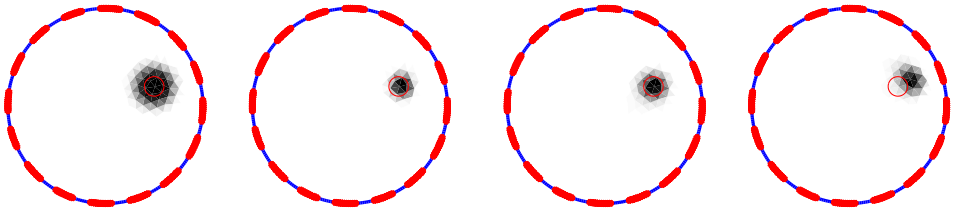

Figure 7: Monte Carlo estimates (10000 samples) of the posterior expectation. In the case where each of the variables $\mathbf{c}, r$ and t are unknown the sampler does not find the right values of r and t (1st from left). If the value of either r (2nd) or t (3rd) is fixed to its true value, the iteration converges close to the exact solution. The anomaly is clearly dislocated in the case where the forward problem is solved only through the linear approximation (24) (4th).

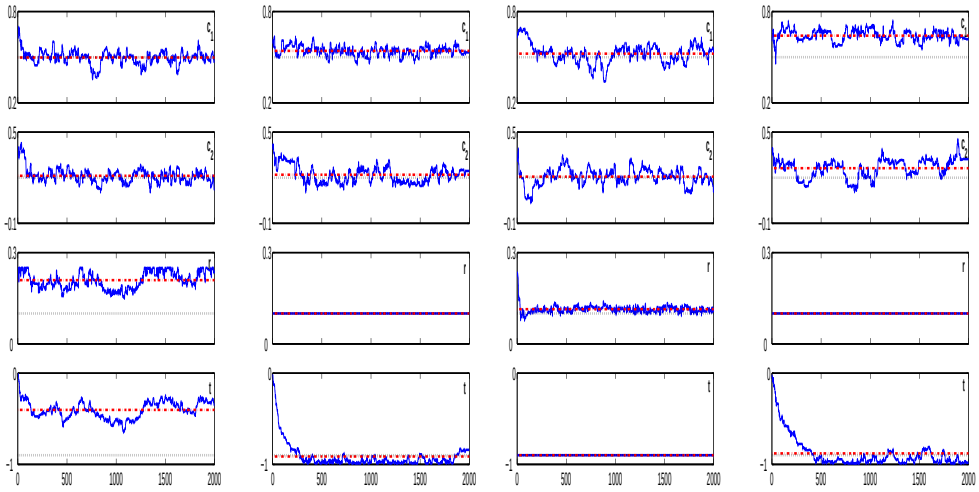

Figure 8: The first 2000 iteration steps of the random-walk Metropolis runs that correspond to the four Monte Carlo approximations illustrated in Figure 7. Behaviour of the unknowns c_1, c_2, r and t are illustrated separately. The black dashed line shows the true value of each of the unknowns. The red dash-dot line shows the Monte Carlo approximation computed from the sample set.

where the product $\begin{pmatrix} 0 & \mathcal{C} \end{pmatrix} Z^d_{\sigma_{bg}}$ can be calculated in advance. It is easy to see that in this case the computational effort is largely determined by the effort of evaluating $(I + tV_d^T Z^d_{\sigma_{bg}} \Lambda_d)^{-1}$.

5.3.3 The sampling plan

The sampling plan is straightforward. We choose $\sigma^{(0)} = \sigma_{bg} = 1$. Since σ_{bg} is known to be close to the exact distribution, we neglect the *burn-in phase*, i.e. iteration steps taken before the chain has reached the important parts of the posterior distribution. The samples $\{\sigma^{(1)}, \ldots, \sigma^{(m)}\}$ are generated in a single long run accepting all the generated samples.

The applied algorithm is the random-walk Metropolis. Since we do not have much information about the structure of the posterior density, the proposal is chosen to be spherically symmetric Gaussian distribution similarly as in algorithm 3.2, i.e. the proposal distribution is $\mathcal{N}(0, \gamma_T^2 I)$, where I is 4×4 identity matrix. Apart from the fact that the acceptance rate is usually controlled by varying the step size, in our implementation the variance of the proposal density is fixed ($\gamma_T^2 = 4 \cdot 10^{-4}$) and the acceptance rate is controlled by choosing the variance of the likelihood density ($\gamma_N^2 \in [2 \cdot 10^{-4}, 10^{-3}]$ in (14)) so that the acceptance rate is close to 35%. Total number of iterations is 10000 in each sampling run.

Additionally, feasibility of the surrogate transition method is experimented by solving the forward problem instead of (11), only through the linearized model

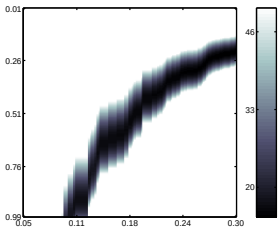

Figure 9: A pseudocolor plot of $|\ln \pi_{lh}(\sigma|\mathbf{V})|$ restricted to the rt-plane. The darkened part of the image shows where $|\ln \pi_{lh}(\sigma|\mathbf{V})| < 50$. The difference between the pictures is hardly notable.

(24) by employing σ_{bg} as an initial guess. In this demonstrative case, the Sherman-Morrison-Woodbury formula works so well, that (24) is actually much slower way to solve the boundary potentials. In cases, where the sampler perturbs the conductivity distribution more globally, the surrogate transition method can, however, be of great importance.

5.3.4 Results

Results of four different random-walk Metropolis runs are plotted in Figures 7 and 8.

The results show that when each of $\mathbf{c}$, r and t are unknown the true values of t and r are not found. This is due to the fact that the inverse problem is outstandingly ill-conditioned in the rt-plane (i.e. the plane, where the center of the anomaly is fixed). That is, various combinations of r- and t-values result in electrode voltages very close to the measured voltage values. Figure 9 shows that the posteriori density does not have one distinct maximum in the rt-plane.

The statistical model yields fairly reasonable solutions provided that either r or t is fixed to its true value. Yet, the anomaly is clearly dislocated if $\mathbf{U}(\sigma)$ is replaced with the surrogate solution $\mathbf{U}^*(\sigma)$.

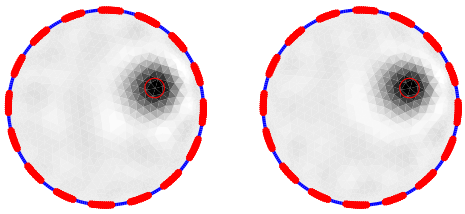

Figure 10: Two quasi-Newton reconstructions with respect to two different weighing matrices both computed as a Monte Carlo approximation (500 samples) of (22).

5.4 The enhanced likelihood model

Estimates of the integrals (20), (21) and (22) are computed as Monte Carlo approximations with respect to a set of 500 independent random samples

$$\{\sigma^{(1)}, \ldots, \sigma^{(500)}\}$$

drawn from the prior distribution described in section 5.3.1. The prior density is a product of uniform densities and, therefore, we can draw independent random samples directly from the prior. Consequently, there is no need to employ MCMC integration. Again, independency of the samples guarantees that the estimates converge quite rapidly. In this case, a set of a few hundred samples seems to be large enough. Similarly as in the previous computations, $\mathbf{U}(\sigma)$ in the estimated equations is obtained by solving the numerical forward problem (11) with respect to the triangulation $\mathcal{T}_h$.

5.4.1 The quasi-Newton reconstruction

Weighing the least-squares norm with the inverse of the conditional covariance matrix (22) is experimented with a slightly modified version of the quasi-Newton iteration. The Hessian matrix (18) is computed by using the Monte Carlo approximation of (22) as a weight matrix but the gradient (19) is, however, weighed with the identity matrix. For some reason, computing the gradient by using (22) decreases the quality of the reconstructions.

Similarly as in the section 5.2, the reconstruction is computed by performing just one step of the iteration using the background conductivity σ_{bg} as an initial guess.

5.4.2 MCMC integration

The enhanced likelihood model is applied to improve the statistical solutions obtained through surrogate forward solution (24). That is, the likelihood density

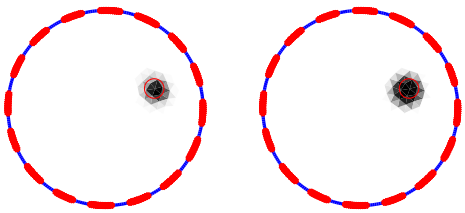

Figure 11: Two Monte Carlo approximations (10000 samples) of the posteriori expectation obtained by employing the enhanced likelihood model and the surrogate forward solution (24). The anomaly is found if either r (left) or t (right) is fixed to its true value.

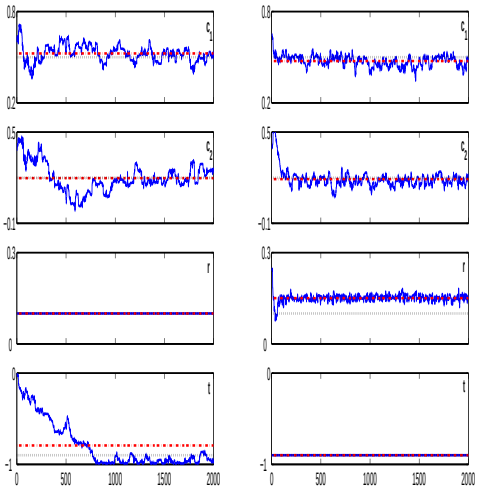

Figure 12: The first 2000 iteration steps of the random-walk Metropolis runs that correspond to the Monte Carlo approximations illustrated in Figure 11. Behaviour of the unknowns c_1, c_2, r and t are illustrated separately. The black dashed line shows the true value of each of the unknowns. The red dash-dot line shows the Monte Carlo approximation computed from the sample set.

(14) is substituted with

$$\pi_{lh}(\mathbf{V} \mid \sigma) \propto \exp\Big(-\frac{1}{2}(\mathbf{U}^*(\sigma) - \mathbf{V} - \mu)^T \Gamma^{-1} (\mathbf{U}^*(\sigma) - \mathbf{V} - \mu)\Big), \qquad (41)$$

where μ and Γ are computed as Monte Carlo approximations of (20), (21) and $\mathbf{U}^*(\sigma)$ is the surrogate forward solution.

The sampling plan is similar to the one introduced in the section 5.3 but this time we examine only the case where the forward problem is solved through (24) with either r or t fixed to its true value.

5.4.3 Results

The quasi-Newton reconstructions corresponding to two different Monte Carlo approximations of (22) are plotted in Figure 10. In both cases the regularization parameters α in (18) and (19) and k in (37) are equal to one. We see that the location of the anomaly is found quite accurately and the overall variation of the solution is on much lower level than in the reconstructions in Figure 5.

Two statistical solutions and the corresponding Markov Chain runs are plotted in Figures 11 and 12. This time the anomaly is found even though the forward solution is only approximated as (24).

6 Discussion

In the numerical experiments, both least-squares approach and the MCMC based estimation scheme succeed rather well in locating the anomaly, that is, in finding $\mathbf{c}$, but the two other sought quantities r and t remain uncertain.

It is evident that the more one has prior knowledge of σ the more preferable is the MCMC approach. Prior information can more easily be decoded into the prior distribution than the regularizing functional. Implementing the quasi-Newton algorithm by applying any regularization method favoring discontinuous conductivities, such as anomalies of certain size and shape, is problematic, since the quasi-Newton assumes differentiability of the map $\sigma \to \Psi(\sigma)$. Again, obtaining any confidence intervals of the quasi-Newton reconstruction is difficult since there is no strict statistical interpretation of the method. Therefore, achieving a feasible least-squares estimate is more or less art of fixing the free-floating parameters so that the outcome is close to the optimal. The result is often a compromise between smoothness and resolution. In our experiments, the quasi-Newton reconstruction is comparable to the MCMC based conditional mean estimate as far as both r and t are unknown. Only assuming that the true value of either of these quantities was known beforehand caused a distinct difference between them.

Due to the fact that the posterior distribution is 'banana shaped' in the rt-plane as illustrated in Figure 9 the random proposal tends to waste a lot of effort a lot of effort exploring the distribution in wrong directions. It is apparent that the shape is likely to be even more awkward in cases where the background conductivity σ_{bg} is not a constant function. For that reason, it is not obvious whether the random-walk Metropolis would be an applicable algorithm for finding an anomaly in such cases. It seems possible that one might need an algorithm that can be adapted to follow both the local and the global dynamics of the posterior distribution. Monte Carlo methodology involves various sophisticated sampling schemes that might turn out to be usable when developing further the present random-walk idea. These include *multipoint methods* [31], *simulated annealing* [23] and *dynamic weighting* [40]. Adaptive Monte Carlo methods have been considered also in [27] and [14].

Besides the Metropolis-Hastings algorithm, one of the most frequently employed transition rules is the *Gibbs sampler* [12]. Metropolis-Hastings is based on 'trial-and-error' strategy whereas the Gibbs sampler is a conditional sampling technique where no rejection is incurred at any of its sampling steps. The transition rules are built upon conditional distributions derived from the target distribution. Thus, there is no problem of finding a suitable proposal function. This algorithm is, however, often successful with complicated target densities. The Gibbs sampler has not been implemented in this study, which is largely due to the difficulties that occurred in connection with drawing random samples from conditional distributions. This is typical in Bayesian computations where the

variance of the target distribution is often very small. More detailed discussion of applying the Gibbs sampler to EIT can be found in [19].

Since the conductivity distribution is updated only in the region of interest, the forward solution is easily obtained by employing the Sherman-Morrison-Woodbury –formula. More global updates would require more expensive methods of linear algebra. Since computational cost of the surrogate forward solution (24) is independent from the structure of σ, it is important to study whether it would be advantageous to use it as a substitute for the solution of (11) or in generating surrogate Markov chains. Figures 7 and 8 indicate that employing the surrogate solution as a pure substitute diminishes the accuracy of the posterior expectation estimate considerably. The anomaly is distinctly dislocated even though its size is given. Applying a surrogate Markov chain that does not locate the anomaly correctly does not seem a feasible idea: each time the actual chain would come close to the true location, the surrogate chain would be likely to drift away from it.

Comparing Figure 5 to Figure 10 and Figure 7 to Figure 11 we see that the use of the enhanced likelihood model improves considerably both the quasi-Newton reconstruction and quality of the approximation (24). Particularly interesting is that the anomaly is correctly located in figure 11. Therefore, there is reason to believe that constructing a surrogate Markov chain transition rule through a combined use of (24) and the enhanced likelihood model might still, be a feasible idea.

A robust model for the inverse problem described in section 5.1 can be obtained by writing the equation (1) as

$$\nabla \cdot (\sigma_{bg} + \delta)\nabla(u_{bg} + u_\delta) = 0, \tag{42}$$

where δ and u_δ are the unknown quantities and $\nabla \cdot \sigma_{bg} \nabla u_{bg} = 0$. Since the support of the anomaly is restricted to a small subset of Ω, it is obvious that δ does not affect remarkably the current field in Ω. In other words, $\nabla u_\delta \approx c \nabla u_{bg}$, where c is some scalar-valued function. Substitution to (42) plus a slight manipulation gives

$$\Delta u_\delta \approx -\frac{1+c}{\sigma_{bg}} \nabla \cdot \delta \nabla u_{bg}, \tag{43}$$

where σ_{bg} has been treated as a scalar-valued constant. From (43) we see that the potential field u_δ is approximately induced by a small supported electromagnetic field $\delta \nabla u_\delta$. That is, the present inverse problem is analogous to detecting an electromagnetic dipole with unknown location, length and charge from a vacuum cavity based on voltage measurements on the boundary, which is evidently an ill-conditioned problem due to the fact that both varying the length and the charge result in very similar changes far from the dipole. In contrast to the charge, the length has a slight effect on the shape of the potential distribution on the boundary and, therefore, one should be able to distinguish these changes. This is

certainly not possible if the number of voltage measurements is too small. Again, the number of injected currents is closely related to the oscillation frequency of ∇u_{bg}, that on the basis of the right hand side of (43) reflects the resolution of the installation. Consequently, the number of electrodes apparently affects the accuracy of the numerical solutions. However, it is also apparent that the present inverse problem would remain ill-conditioned in rt-plane even though the number of electrodes was increased.

Finally, it is important to point out that the approximation error (34) is large compared to the measurement error (33). Unfortunately, the limited memory capacity of the available computer hardware did not allow significant refinements of the triangulation. Refining the triangulation would certainly reduce (34) but then again each triangulation has its maximal resolution. In other words, for any triangulation there are anomalies for which (34) is large. Thus, the case we have studied indeed tells us about what happens when the anomaly is small in terms of the resolution of the triangulation. Another topic would be to examine the case where the measurement error is the dominating one.

7 Summary and Conclusions

The findings and conclusions of this study can be formulated as follows.

- It was found that a regularization method favoring smooth solutions can be produced effectively by using the finite element method as described in section 5.2.2.

- Even though it is difficult to construct a regularization method favoring arbitrary conductivities (e.g. strongly discontinuous conductivities), the statistical model is preferable to the least-squares approach only if prior knowledge accurate enough is available.

- MCMC based estimation model was superior if either the size or the value of conductivity of the anomaly was given.

- Solving the forward problem by applying the finite element method led into statistical solutions that were considerably better than those obtained by applying the surrogate forward solution.

- The enhanced likelihood model improved significantly both the least-squares reconstruction and workability of the surrogate solution.

- The seemingly primitive problem demonstrated in the present experiments turned out to be difficult to solve. Therefore, further numerical analysis would be a natural continuation of the study.

References

[1] Ammari H, Beretta E, Francini E 2004 Reconstruction of thin conductivity imperfection, *Applicable Analysis* **83**: 63–76

[2] Andersen K, , Brooksz S P and Hansen M B 2001 A Bayesian Approach to Crack Detection in Electrically Conducting Media *Inverse Problems* **17**:121–136

[3] Beretta E, Francini E, Vogelius M 2003 Asymptotic formulas for steady state voltage potentials in the presence of thin inhomogeneities. A rigorous error analysis *J. Math. Pures Appl.* **82**(10):1277–1301

[4] Braess D 2001 *Finite Elements* (Cambridge : Cambridge University Press)

[5] Brown B, Barber D and Seagar A 1985 Applied potential tomography: possible clinical applications *Clin. Phys. Physiol. Meas.* **6**:109–21

[6] Cheney A P 1980 *On an inverse boundary value problem Seminar on numerical analysis and its applications to continuum physics* (Rio de Janeiro : Soc. Brasileira de Matematica) p. 65-73

[7] Cheney M and Isaacson D 1992 Distinguishability in impedance imaging *IEEE Trans. Biomed. Eng.* **39**:852–860

[8] Cheney M, Isaacson D, Newell J 1999 Electrical impedance tomography *SIAM Review* **41**:85–101

[9] Cherepenin V A, Karpov A Y, Korjenevsky A V, Kornienko V N, Kultiasov Y S, Ochapkin M B, Trochanova O V, and Meister J D 2002 Three-dimensional EIT imaging of breast tissues: system design and clinical testing *IEEE Transactions on Medical Imaging* **21**:662–667

[10] Clay M T and Ferree T C 2002 Weighted regularization in electrical impedance tomography with applications to acute cerebral stroke *IEEE Transactions on Medical Imaging* **21**:629–637

[11] Dickin F and Wang M 1996 Electrical resistance tomography for process applications *Measurement Science and Technology* **7**:247–260

[12] Geman S and Geman D 1984 Stochastic relaxation, Gibbs distributions and the Bayesian restoration of images. *IEEE Transactions on Pattern Analysis and Machine Intelligence* **6**:721–741

[13] Golub G and van Loan C 1989 *Matrix Computations* (Baltimore : The John Hopkins University Press)

[14] Haario H, Saksman E and Tamminen J 2001 An adaptive Metropolis algorithm *Bernoulli* **7**(2): 223–242

[15] Hartov A, Soni N K, and Paulsen K D 2004 Variation in breast EIT measurements due to menstrual cycle *Physiological Measurement* **25**:295–299

[16] Hastings W K 1970 Monte Carlo sampling methods using Markov chains and their applications *Biometrika* **57**(1):97–109

[17] Heikkinen L M, Leinonen K, Kaipio J P, Vauhkonen M and Savolainen T 2001 Electrical process tomography with known internal structures and resistivities *Inverse Problems* **21**:431–454

[18] Isaacson D 1993 Distinguishability of conductivities by electric current computed tomography *IEEE Trans. Biomed. Eng.* **40**:1328–1330

[19] Kaipio J P, Kolehmainen V, Somersalo E and Vauhkonen M 2000 Statistical inversion and Monte Carlo sampling methods in electrical impedance tomography *Inverse Problems* **16**:1487–1522

[20] Kaipio J P and Somersalo E 2004 *Statistical and Computational Methods for Inverse Problems* (Berlin: Springer)

[21] Kaup P G, Santosa F and Vogelius M 1996 Method of imaging corrosion damage in thin plates from electrostatic data *Inverse Problems* **12**:279–293

[22] Kerner T E, Paulsen K D, Hartov A, Soho S K and Poplack S P 2002 Electrical impedance spectroscopy of the breast: clinical imaging results in 26 subjects *IEEE Transactions on Medical Imaging* **21**:638–645

[23] Kirkpatrick S, Gelatt C D and Vecci M P 1983 Proceedings of the national academy of sciences of USA *Science*, **220**:671–680

[24] Liu J S and Chen R 1998 Sequential monte carlo methods for dynamic systems *Journal of the American Statistical Association* **93**(443):1032–1044

[25] Liu J S 2001 *Monte Carlo Strategies in Scientific Computing* (Berlin: Springer)

[26] Metropolis M, Rosenbluth A W, Rosenbluth M N, Teller A H and Teller E 1953 Equations of state calculations by fast computing machines *Journal of Chemical Physics* **21**(6):1087–1091

[27] Mira A 2001 Ordering and improving the performance of Monte Carlo markov chains *Statist. Sci.* **16**(4):340–350

[28] Mueller J Isaacson D and Newell J 1999 A reconstruction algorithm for electrical impedance tomography data collected on rectangular electrode arrays *IEEE Trans. Biomed. Eng.* **46**:1379–1386

[29] Nummelin E 1984 *General Irreducible Markov Chains and Non-negative Operators* (Cambridge: Cambridge University Press)

[30] Polydorides N Lionheart W R and McCann H 2002 Krylov subspace iterative techniques: on the detection of brain activity with electrical impedance tomography *IEEE Transactions on Medical Imaging* **21**:596–603

[31] Quin Z and Liu J 2001 Multipoint Metropolis method with application to hybrid Monte Carlo *Journal of Computational Physics* **172**:827–840

[32] Stanley S J, Mann R, Primrose K 2002 Tomographic imaging of fluid mixing in 3-d for single-feed semi-batch operation of a stirred vessel *Trans. IchemE* **80**(A):903–909

[33] Roberts G O, Gelman A and Gilks W R 1997 Weak convergence and optimal scaling for random walk metropolis algorithms *Annals of Applied Probability* **7**:110–120

[34] Seppänen A, Heikkinen L M, Savolainen T, Somersalo E and Kaipio J P 2003 An experimental evaluation of state estimation with fluid dynamical models in process tomography *Proceedings of 3rd world congress on industrial process tomography*, vol 1, p 541

[35] Seppänen A, Vauhkonen M, Vauhkonen P J, Somersalo E and Kaipio J P 2001 State estimation with fluid dynamical evolution models in process tomography - an application to impedance tomography *Inverse Problems* **17**:467–483

[36] Somersalo E, Cheney M and Isaacson D 1992 Existence and uniqueness for electrode models for electric current computed tomography *SIAM J. Appl. Math.* **52**:1023–1040

[37] Vauhkonen M 1997 Electrical Impedance Tomography and Prior Information *PhD thesis*, University of Kuopio, Kuopio, Finland

[38] Vilhunen T, Heikkinen L M, Savolainen T, Vauhkonen P J, Lappalainen R, Kaipio J P, and Vauhkonen M 2002 Detection of faults in resistive coatings with an impedance-tomography-related approach *Measurement Science and Technology* **13**:865–872

[39] Wang W, Tang M, McCormick M and Dong X 2001 Preliminary results from an EIT breast imaging simulation system *Physiological Measurement* **22**:39–48

[40] Wong W and Liang F 1997 Proceedings of the national academy of sciences of USA *Journal of Computational Physics* **94**(26):14220–14224

(continued from the back cover)

A479 Jarmo Malinen
Conservativity of Time-Flow Invertible and Boundary Control Systems
December 2004

A478 Niko Marola
Moser's Method for minimizers on metric measure spaces
October 2004

A477 Tuomo T. Kuusi
Moser's Method for a Nonlinear Parabolic Equation
October 2004

A476 Dario Gasbarra , Esko Valkeila , Lioudmila Vostrikova
Enlargement of filtration and additional information in pricing models: a Bayesian approach
October 2004

A475 Iivo Vehviläinen
Applyining mathematical finance tools to the competitive Nordic electricity market
October 2004

A474 Mikko Lyly , Jarkko Niiranen , Rolf Stenberg
Superconvergence and postprocessing of MITC plate elements
January 2005

A473 Carlo Lovadina , Rolf Stenberg
Energy norm a posteriori error estimates for mixed finite element methods
October 2004

A472 Carlo Lovadina , Rolf Stenberg
A posteriori error analysis of the linked interpolation technique for plate bending problems
September 2004

A471 Nuutti Hyvönen
Diffusive tomography methods: Special boundary conditions and characterization of inclusions
April 2004

HELSINKI UNIVERSITY OF TECHNOLOGY INSTITUTE OF MATHEMATICS
RESEARCH REPORTS

The list of reports is continued inside. Electronical versions of the reports are available at *http://www.math.hut.fi/reports/* .

A485 Sampsa Pursiainen
Bayesian approach to detection of anomalies in electrical impedance tomography
April 2005

A484 Visa Latvala , Niko Marola , Mikko Pere
Harnack's inequality for a nonlinear eigenvalue problem on metric spaces
March 2005

A482 Mikko Lyly , Jarkko Niiranen , Rolf Stenberg
A refined error analysis of MITC plate elements
April 2005

A481 Dario Gasbarra , Tommi Sottinen , Esko Valkeila
Gaussia Bridges
December 2004

A480 Ville Havu , Jarmo Malinen
Approximation of the Laplace transform by the Cayley transform
December 2004

ISBN 951-22-7637-2
ISSN 0784-3143